Proceedings of GT2007
ASME Turbo Expo 2007: Power for Land, Sea and Air
May 14–17, 2007, Montreal, Canada

GT2007-28065

ADDITIONAL INVESTIGATIONS INTO THE NATURAL FREQUENCIES AND CRITICAL SPEEDS OF A ROTATING, FLEXIBLE SHAFT-DISK SYSTEM

Lyn M. Greenhill and Valerie J. Lease
DynaTech Engineering, Inc., Roseville, CA 95661

ABSTRACT

Traditional rotor dynamics analysis programs make the assumption that disk components are rigid and can be treated as lumped masses. Several researchers have studied this assumption with specific analytical treatments designed to simulate disk flexibility. The general conclusions reached by these studies indicated disk flexibility has little effect on critical speeds but significantly influences natural frequencies. This apparent contradiction has been reexamined by using axisymmetric harmonic finite elements to directly represent both disk and shaft flexibility along with gyroscopic effects. Results from this improved analysis show that depending on the thickness-to-diameter (slenderness) ratio of the disk and the axial position of the disk on the shaft, there are significant differences in all natural frequencies, for both forward and backward modes, including synchronous crossings at critical speeds.

INTRODUCTION

Intuitively, the interaction between a flexible disk and elastic shaft must be important, yet this coupling is largely ignored in rotor dynamic analysis. There have been numerous studies of rotor models in which the effects of disk flexibility have been included. The conclusions of these investigations are somewhat conflicting, in that the effect may be significant for certain geometry and natural frequencies.

One of the early and noteworthy analyses was conducted by Chivens and Nelson [1]. They formulated a set of system equations that coupled the disk and shaft motion and obtained closed form solutions using the Laplace transforms for various geometries. Their two general conclusions were that natural frequencies are significantly affected by disk flexibility, however, critical speeds are not. This rather surprising finding has been cited as a justification for the practice of lumping disk mass properties at nodes in rotor dynamic beam models.

Dopkin and Shoup [2] examined disk flexibility effects on rotating shaft natural frequencies using modified transfer matrices. Their results showed a significant reduction in resonant frequencies, mostly at low speeds, confirming the natural frequency conclusions of Chivens and Nelson.

Brémand, Ferraris, and Lalanne [3] developed a finite element representation of a flexible disk system with harmonic displacements, which coupled shaft bending and disk motion. Using a model of a typical industrial gas turbine, they showed a decrease in critical speeds of the system using a flexible disk.

Vance [4] studied disk flexibility with several rotor configurations, performing experimental and analytical investigations primarily for agreement with modal testing. His analytical model incorporated the effects of disk flexibility using an approximate transfer matrix procedure based bending of a circular plate similar to Dopkin and Shoup. Vance's studies showed that the use of disk flexibility could improve the correlation between experimental and calculated free-free natural frequencies.

Flowers [5] performed a detailed finite element analysis of shaft-disk flexibility using a combination of beam elements for the shaft and 3D solids for the disks. His conclusions are very similar to Vance's, in that the inclusion of disk flexibility can significantly alter the free-free modes of a rotor assembly.

While the use of general purpose finite element models to represent flexible shaft-disk systems is perfectly acceptable for free-free mode calculations, this approach does not include a fundamental analysis consideration crucial to rotor dynamics – gyroscopic effects. The existing beam formulations of rotor dynamic analysis, such as with transfer matrices as used by Vance, or finite elements as described by Greenhill, Nelson, and Bickford [6], do include gyroscopic considerations but cannot fundamentally include flexible disks. To accurately predict the influence of rotation on a shaft-disk system, and directly incorporate disk flexibility, a specialized finite element formulation is required.

The most relevant approach to the shaft and disk flexibility problem was developed by Stephenson and Rouch [7] with an axisymmetric harmonic formulation. In addition to the standard mass and stiffness matrices that can be obtained from references such as Cook, et al [8], they developed a kinetic energy based gyroscopic matrix. Because these finite elements include both radial and axial deformations, the representation of disk flexibility is inherent.

Using the Stephenson and Rouch formulation, the original conclusions reached by Chivens and Nelson are re-examined in this paper. A specialized rotor dynamic analysis program using the axisymmetric harmonic elements has been developed and applied to equivalent geometry. The results from these calculations are discussed in this paper.

ANALYSIS DESCRIPTION

The axisymmetric harmonic finite element allows a structure with an axis of symmetry to be subjected to non-axisymmetric loads and deflections. A 2D representation of the structure, in the radial and axial directions, is needed for the formulation. The circumferential coordinate is intrinsic, since each element can be thought of as a complete ring. For the non-symmetric loading and deflection, a Fourier series is used, in which the superposition of each harmonic solution provides the total response. The solid cross-section displacements are defined by sine and cosine Fourier series,

$$u(r,z) = \sum_{m=0}^{\infty} u_{mS}\cos m\theta + \sum_{m=0}^{\infty} u_{mA}\sin m\theta \qquad (1)$$

$$v(r,z) = \sum_{m=0}^{\infty} v_{mS}\cos m\theta + \sum_{m=0}^{\infty} v_{mA}\sin m\theta \qquad (2)$$

$$w(r,z) = \sum_{m=0}^{\infty} w_{mS}\sin m\theta - \sum_{m=0}^{\infty} w_{mA}\cos m\theta \qquad (3)$$

in the radial, axial, and tangential directions. For the lateral bending of a shaft, the only harmonic mode of interest is $m = 1$.

Generating the element stiffness matrix starts with an integral expression for potential energy,

$$P = \tfrac{1}{2}\int_V \{\sigma\}^T\{\varepsilon\}\, dV \qquad (4)$$

where the stress $\{\sigma\}$ and strain $\{\varepsilon\}$ vectors in (4) are given by,

$$\{\sigma\}^T = \{\sigma_r \;\; \sigma_z \;\; \sigma_\theta \;\; \tau_{rz} \;\; \tau_{z\theta} \;\; \tau_{r\theta}\} \qquad (5)$$

$$\{\varepsilon\}^T = \{\varepsilon_r \;\; \varepsilon_z \;\; \varepsilon_\theta \;\; \gamma_{rz} \;\; \gamma_{z\theta} \;\; \gamma_{r\theta}\} \qquad (6)$$

In cylindrical coordinates, the strain-displacement relationship is defined as,

$$\{\varepsilon\} = [\partial]\{d\}$$

$$[\partial] = \begin{bmatrix} \partial/\partial r & 0 & 0 \\ 0 & \partial/\partial z & 0 \\ 1/r & 0 & (\partial/\partial\theta)/r \\ \partial/\partial z & \partial/\partial r & 0 \\ 0 & (\partial/\partial\theta)/r & \partial/\partial z \\ (\partial/\partial\theta)/r & 0 & (\partial/\partial r - 1/r) \end{bmatrix} \qquad (7)$$

The stress and strain vectors in (5) and (6) are related by,

$$\{\sigma\} = [D]\{\varepsilon\} \qquad (8)$$

where the constitutive matrix $[D]$ in (8) is expressed as, assuming isotropic materials,

$$[D] = \frac{E(1-\nu)}{(1+\nu)(1-2\nu)} \begin{bmatrix} 1 & F & F & 0 & 0 & 0 \\ & 1 & F & 0 & 0 & 0 \\ & & 1 & 0 & 0 & 0 \\ & & & H & 0 & 0 \\ & sym & & & H & 0 \\ & & & & & H \end{bmatrix} \qquad (9)$$

$$F = \frac{\nu}{(1-\nu)} \qquad H = \frac{(1-2\nu)}{2(1-\nu)}$$

in which ν is the poisson ratio. Rewriting the potential energy in (4) in terms of matrix expressions from (8) and (9),

$$P = \tfrac{1}{2}\int_V \left([D][\partial]\{d\}\right)^T \cdot [\partial]\{d\}\, dV \qquad (10)$$

and noting that the element displacement is related to the nodal displacements through the shape functions [N], the terms in equation (10) can be rewritten,

$$\begin{aligned}[\partial]\{d\} &= [\partial][N]\{q\} \\ &= \left[\, [\partial][N_S] \,\vdots\, [\partial][N_A] \,\right]\{q\} \\ &= [B]\{q\}\end{aligned} \tag{11}$$

in which [B] is strain-displacement matrix, a product of the shape functions and the partial derivatives in (7), defined as,

$$\begin{aligned}[B] &= \left[\, [B_S] \,\vdots\, [B_A] \,\right] \\ [B_S] &= [\partial][N_S] \text{ and } [B_A] = [\partial][N_A]\end{aligned} \tag{12}$$

where [N_S] and [N_A] are the shape function matrices for the symmetric and anti-symmetric response components. Expressions for the shape functions depend on the element selected, and in this work, quadratic quadrilaterals were used (see Cook, et al [7]). It should be noted that bi-linear quadrilaterals would be inappropriate to represent lateral bending.

Using the notation of (11) and (12), the potential energy expression in (10) can be further arranged and written in terms of nodal displacements as,

$$P = \tfrac{1}{2}\int_V \{q\}^T [B]^T [D]\, [B]\{q\}\, dV \tag{13}$$

which allows the element stiffness matrix to be written by inspection from equation (13) as,

$$\begin{aligned}[K_e] &= \int_V [B]^T [D]\, [B]\, dV \\ &= \int_z \int_r \int_\theta [B]^T [D]\, [B]\, r\, d\theta\, dr\, dz\end{aligned} \tag{14}$$

Factoring (14) and using the relationships in (12) allows an alternate expression for the stiffness matrix to be written,

$$\begin{aligned}[K_e] &= \int_V \begin{bmatrix} [B_S]^T \\ \hdashline [B_A]^T \end{bmatrix} \left[\, [D][B_S] \,\vdots\, [D][B_A] \,\right] dV \\ &= \int_V \begin{bmatrix} [B_S]^T [D]\, [B_S] & \vdots & [B_S]^T [D]\, [B_A] \\ \hdashline [B_A]^T [D]\, [B_S] & \vdots & [B_A]^T [D]\, [B_A] \end{bmatrix} dV\end{aligned} \tag{15}$$

or in terms of matrix expressions,

$$[K_e] = \begin{bmatrix} [K_{SS}] & \vdots & [K_{SA}] \\ \hdashline [K_{AS}] & \vdots & [K_{AA}] \end{bmatrix} \tag{16}$$

By performing the matrix multiplications in equation (15), it can be shown that,

$$\begin{aligned}[K_{SA}] &= [K_{AS}]^T = [0] \\ [K_{AA}] &= [K_{SS}]\end{aligned} \tag{17}$$

and therefore the element stiffness matrix in equation (16) can be written as,

$$[K_e] = \begin{bmatrix} [K_{SS}] & \vdots & [0] \\ \hdashline [0] & \vdots & [K_{SS}] \end{bmatrix} \tag{18}$$

which is to say that symmetric and anti-symmetric components of the element stiffness matrix are equal.

The development for the mass matrix begins with the integral expression for kinetic energy,

$$T = \tfrac{1}{2}\int_V \rho(\dot{u}^2 + \dot{v}^2 + \dot{w}^2)dV = \tfrac{1}{2}\int_V \rho\{\dot{d}\}^{\mathrm{T}}\{d\}dV \tag{19}$$

and noting that,

$$\{d\} = \left[\, [N_S] \,\vdots\, [N_A] \,\right]\begin{Bmatrix}\{d_S\} \\ \{d_A\}\end{Bmatrix} = [N]\{q\} \tag{20}$$

which allows the kinetic energy to be written as,

$$\begin{aligned}T &= \tfrac{1}{2}\{\dot{d}\}^T \int_V \rho \begin{bmatrix} [N_S]^T [N_S] & \vdots & [N_S]^T [N_A] \\ \hdashline [N_A]^T [N_S] & \vdots & [N_A]^T [N_A] \end{bmatrix} dV \{\dot{d}\} \\ &= \tfrac{1}{2}\{\dot{d}\}^T [M_e]\{\dot{d}\}\end{aligned} \tag{21}$$

where the element mass matrix [M_e] is given by,

$$[M_e] = \begin{bmatrix} [M_{SS}] & \vdots & [M_{SA}] \\ \hdashline [M_{AS}] & \vdots & [M_{AA}] \end{bmatrix} \tag{22}$$

By expanding the shape function products in equation (21), it can be shown that,

$$\begin{aligned}[M_{SA}] &= [M_{AS}]^T = [0] \\ [M_{AA}] &= [M_{SS}]\end{aligned} \tag{23}$$

and therefore the element mass matrix in equation (22) can be written as,

$$[M_e] = \begin{bmatrix} [M_{SS}] & \vdots & [0] \\ \hdashline [0] & \vdots & [M_{SS}] \end{bmatrix} \tag{24}$$

which is comparable to the form of the element stiffness matrix with the symmetric and anti-symmetric components equal. As such, only the symmetric submatrix need be retained for use in the assembly of system analysis equations.

The element gyroscopic matrix is derived from the kinetic energy expression, equation (19). Assuming small angles of rotation, dropping second order rotation terms, and ignoring any inertia forces due to constant rotation, the kinetic energy expression can be written as,

$$T = -\Omega \int_V v \frac{d}{dt}\left(-\frac{\partial w}{\partial z}\right) r\rho dV \tag{25}$$

Noting that the axial and tangential displacements are Fourier series represented by equations (1) through (3), equation (25) can be expanded in terms of the circumferential displacement functions for a given harmonic mode. This will result in expressions involving axial displacement and time derivatives of the circumferential partial derivatives similar to equation (15) and (21). These expressions are integrated from $0 \le \theta \le 2\pi$ and then written in terms of the velocities at the element nodes to become,

$$\begin{aligned} T = &-\pi\Omega \int_A \rho r^2 \left[\sum_{i=1}^{n} N_i v_{iS} * \sum_{j=1}^{n} \frac{\partial N_j}{\partial z} \dot{w}_{iA}\right] drdz \\ &+ \pi\Omega \int_A \rho r^2 \left[\sum_{i=1}^{n} N_i v_{iA} * \sum_{j=1}^{n} \frac{\partial N_j}{\partial z} \dot{w}_{iS}\right] drdz \end{aligned} \tag{26}$$

To obtain the gyro matrix, equation (26) must be expanded and then Lagrange's equation is applied, the components of which are,

$$\frac{\partial T}{\partial v_{kS}} = -\pi\Omega \int_A \rho r^2 \left[N_k \sum_{j=1}^{n} \frac{\partial N_j}{\partial z} \dot{w}_{jA}\right] drdz \tag{27}$$

$$\frac{\partial T}{\partial v_{kA}} = +\pi\Omega \int_A \rho r^2 \left[N_k \sum_{j=1}^{n} \frac{\partial N_j}{\partial z} \dot{w}_{jS}\right] drdz \tag{28}$$

$$\frac{d}{dt}\left(\frac{\partial T}{\partial \dot{w}_{kA}}\right) = -\pi\Omega \int_A \rho r^2 \left[\frac{\partial N_k}{\partial z} \sum_{i=1}^{n} N_i \dot{v}_{iS}\right] drdz \tag{29}$$

$$\frac{d}{dt}\left(\frac{\partial T}{\partial \dot{w}_{kS}}\right) = +\pi\Omega \int_A \rho r^2 \left[\frac{\partial N_k}{\partial z} \sum_{i=1}^{n} N_i \dot{v}_{iA}\right] drdz \tag{30}$$

where k = 1,2,…,n with n the number of nodes per element.

Noting that the kinetic energy expressions in equations (27) – (30) have terms multiplying element velocity, the gyroscopic element matrix can be written by inspection as,

$$[G] = \pi\Omega \int_A \rho r^2 [\tilde{G}]\, drdz \tag{31}$$

where the $[\tilde{G}]$ matrix is a skew symmetric combination of shape functions and partial derivatives associated with the velocity terms. Using the definition of the displacement vector from equation (20) the components of $[\tilde{G}]$ are given by,

$$[\tilde{G}] = \left[\begin{array}{c|c} [0] & [G_{SA}] \\ \hline -[G_{SA}]^T & [0] \end{array}\right] \tag{32}$$

which is similar to equations (18) and (24) for stiffness and mass except that the matrix is skew symmetric. This is a necessary and definitive condition for gyroscopic effects. The submatrices in equation (32) are defined as,

$$[G_{SA}] = \begin{bmatrix} [G_{11}] & [G_{12}] & \cdots & [G_{1n}] \\ [G_{21}] & [G_{22}] & \cdots & [G_{2n}] \\ \vdots & \vdots & \vdots & \vdots \\ [G_{n1}] & [G_{n2}] & \cdots & [G_{nn}] \end{bmatrix} \tag{33}$$

where the individual components are 3 x 3 matrices, for any mode number m, expressed as,

$$[G_{jk}] = c\pi\Omega \int_A \rho r^2 \begin{bmatrix} 0 & 0 & 0 \\ 0 & 0 & N_j \dfrac{\partial N_k}{\partial z} \\ 0 & hN_k \dfrac{\partial N_j}{\partial z} & 0 \end{bmatrix} drdz \tag{34}$$

in which the mode number multiplier h is either 0 or 1 and the constant c either 1 or 2, corresponding to,

for $m = 0$, $h = 0$, $c = 2$

for $m \ge 1$, $h = 1$, $c = 1$

The terms in the element stiffness, mass, and gyroscopic matrices in equations (18), (24), and (32) are obtained by numerical integration, and as such, cannot be written directly. Individual element matrices are assembled into system level equations and then solved using first order techniques to obtain natural frequencies and mode shapes.

Displacements at each node, for a given mode shape, will consist of a complex conjugate pair for the symmetric and anti-symmetric components for harmonic modes greater than zero. To resolve these displacements into a meaningful mode shape, the use of elliptical orbit relations such as described in Lund and Orcutt [9] were applied in this analysis.

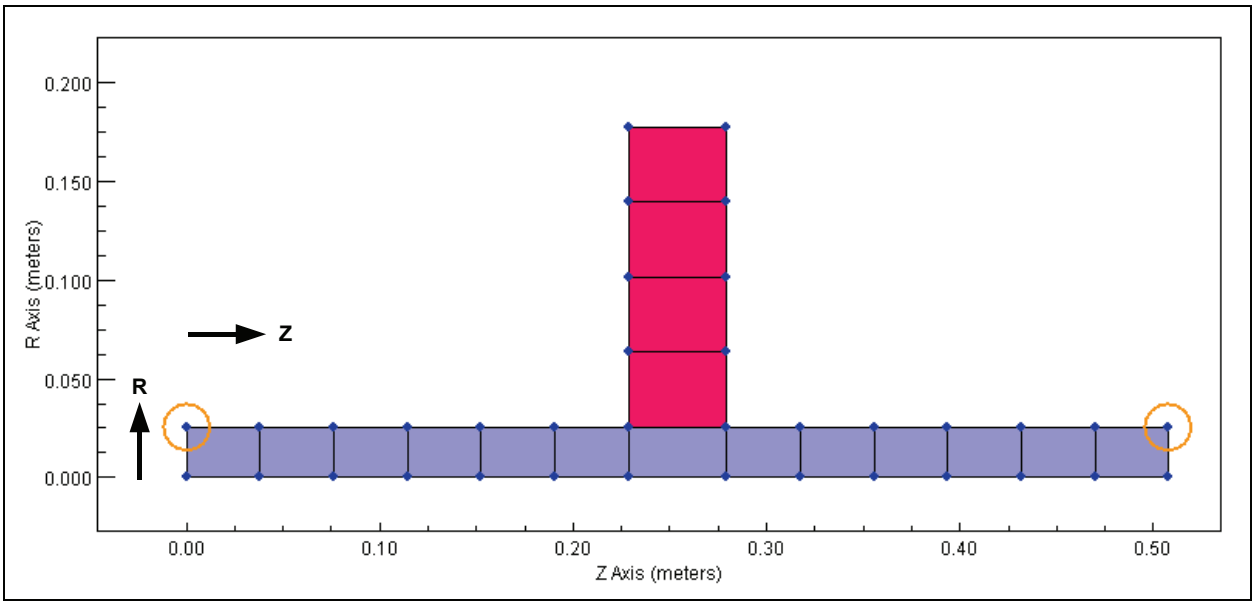

Figure 1. Geometry of Shaft and Disk System, Symmetric Configuration (x/l = 0.5)

RESULTS

To apply the axisymmetric harmonic finite elements to the question of disk flexibility, a typical shaft and disk system was created and analyzed. Each end of the shaft was restrained by a simply supported boundary condition, which constrains radial and axial motion, but allows rotation about the fixed node. This model is identical to what was used in the calculations performed by Chivens and Nelson.

Figure 1 illustrates a typical finite element model and geometry used in this analysis. A total of 17 axisymmetric elements were used, 13 on the shaft and 4 to represent the disk. This level of mesh density was used to obtain reasonable accuracy for the first 3 bending modes. Since low order modes are of the most interest in rotor dynamics, this study only considered the difference in natural frequencies between a rigid and flexible disk for the first three forward modes, since these are thought of as traditional critical speeds. The small circles on the end nodes signify the application of the boundary conditions, and the R (radial) and Z (axial) axes are shown.

There are numerous combinations of parameters that can be investigated with the shaft and disk configuration. However, since the primary objective was to determine if the critical speeds are affected, only the following variables were considered:

- μ, the non-dimensional shaft-plate stiffness parameter
- x/l, the relative disk/shaft location
- b/a, the ratio of disk outer to inner diameter

As the data shows, these parameters are more than sufficient to show the effect of disk flexibility.

To simulate a rigid disk, the modulus of the elements comprising the disk was increased by 3 orders of magnitude from normal. This amount of change was spot checked by using higher values in some of the cases, and it was found that very little difference in the results was obtained.

A total of 5 symmetric (x/l = 0.5) and 2 offset (x/l = 0.25) cases were examined in the analysis. The symmetric cases examined both disk thickness and disk diameter ratio. The offset runs just considered thickness, based on the results from the symmetric examples. With the offset cases, the finite element mesh was changed to reduce the number of elements on the short end of the shaft, and correspondingly increase the number on the long end. The total number of elements remained constant.

Symmetric Disk

With the disk at the center of the shaft, values of μ equal to 0.229, 1.832, and 14.65 were analyzed by changing the disk thickness. These three parameters correspond to a thin, nominal, and thick disk. Two values of b/a equal to 7.0 and 9.0 were considered as well. For reference, Figure 1 illustrates the finite element mesh for μ = 1.832 and b/a = 7.0 which were considered nominal parameters.

Results from the baseline analysis are illustrated in Figure 2, which displays a natural frequency diagram or whirl map for the first three forward modes using the shaft non-dimensional natural frequency βl for the axes scales. The diagonal line in the figure corresponds to synchronous excitation. The implication of this line is that a crossing by a mode is by definition a critical speed.

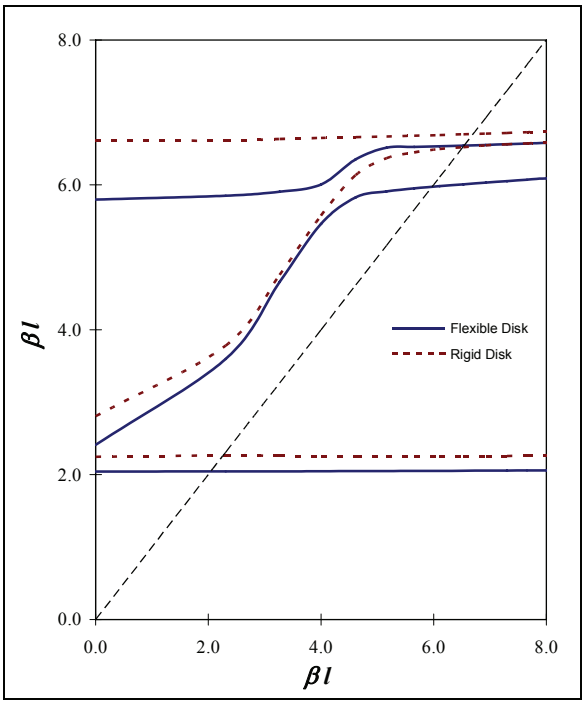

Figure 2. Modes for μ = 1.832, b/a = 7.0, x/l = 0.5

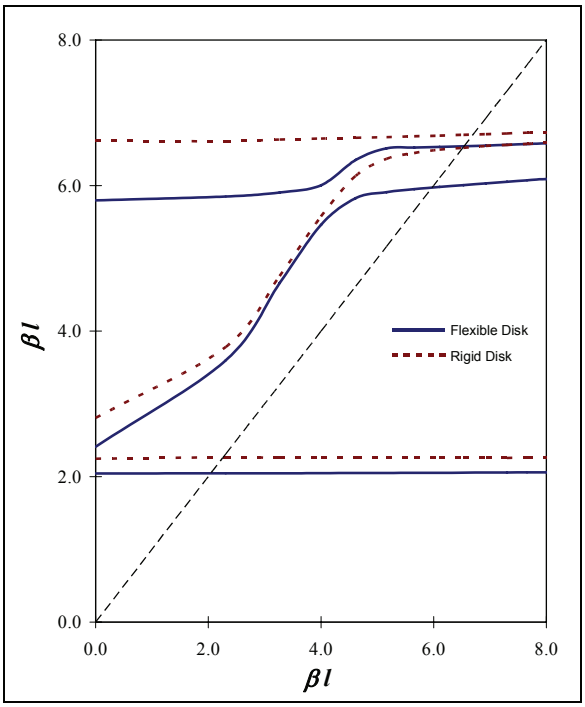

Figure 3. Modes for μ = 14.65, b/a = 7.0, x/l = 0.5

Compared to the results contained in Chivens and Nelson, it is immediately obvious that the natural frequencies do not agree, and more significantly, there is no match of critical speeds either. The largest frequency difference is produced at the second mode, with the rigid disk generating a critical speed that is 19% higher.

Results for the other two cases for a fixed ratio of disk diameter are displayed in Figure 3 for the thick disk and Figure 4 for the thin disk. There is very little different in the plots of the nominal and thick disk, however, there is a pronounced variation in the response with the thin disk. Note that the first mode critical speed is nearly identical and the modes have more abrupt changes in frequency as the speed increases. The greatest frequency difference of 30% between the rigid and flexible disks is obtained with the thin disk at the second mode.

The reason why the second mode shows more difference than the other two is that the disk is pitching and therefore able to exert a moment on the shaft. This moment creates pronounced gyroscopic stiffening displayed in the significant change in frequency as a function of speed. As illustrated in Figure 5, the first and third modes have little rotation of the disk, as it is just translating, while the shaft is bending. Note that with the second mode, there is appreciable disk bending, indicating that disk flexibility will influence natural frequencies.

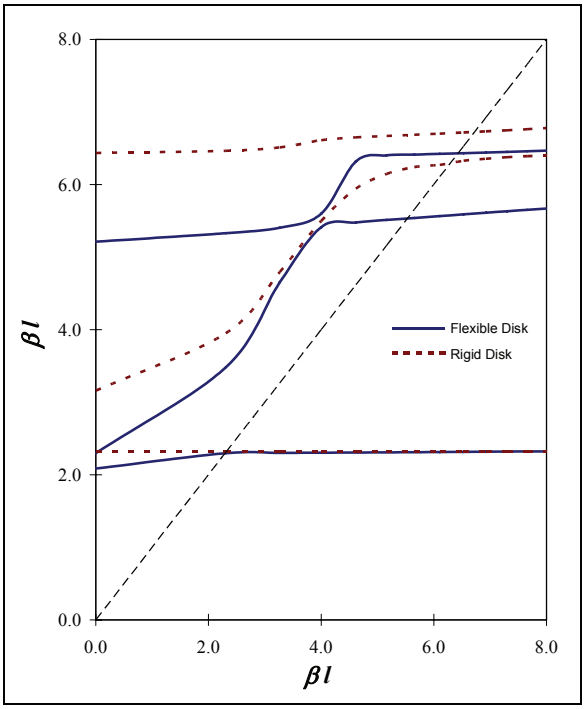

Figure 4. Modes for μ = 0.229, b/a = 7.0, x/l = 0.5

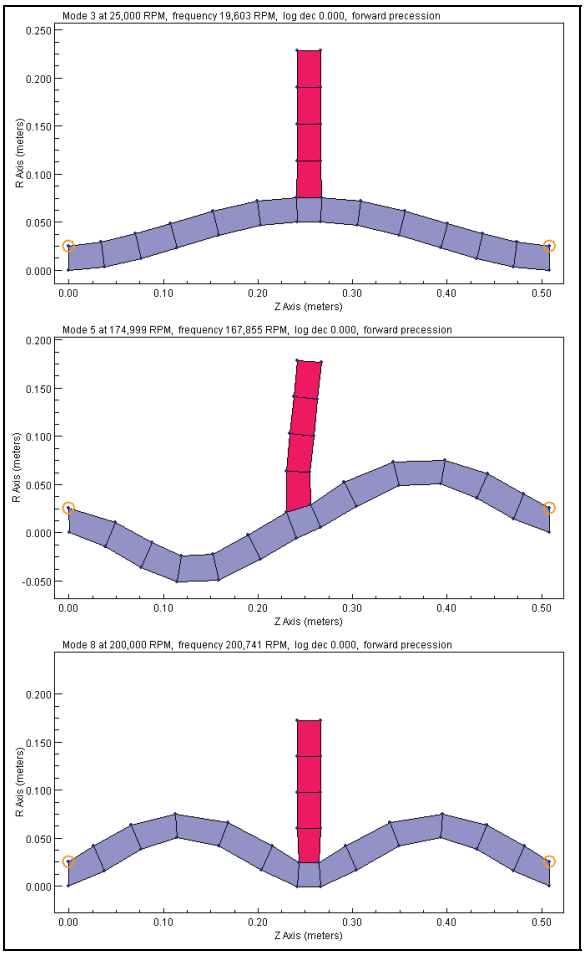

Figure 5. Mode shapes for symmetric disk

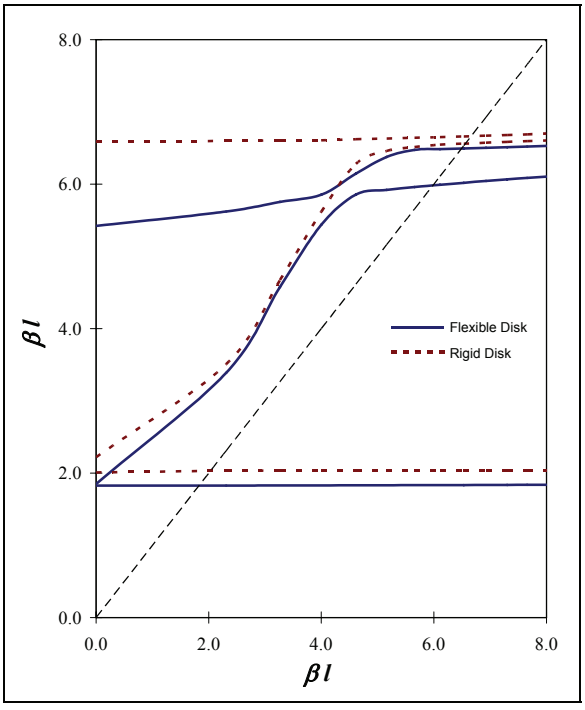

Figure 6. Modes for μ = 1.832, b/a = 9.0, x/l = 0.5

The final case considered with the symmetric disk is illustrated in Figure 6 for a larger disk diameter ratio. As would be expected, this case has more separation between the rigid and flexible critical speeds due to the increased disk mass. Compared with the map in Figure 2, there is 25% difference in the critical speed at the second mode.

It would be an interesting analysis to determine at what disk diameter ratio no difference in the rigid and flexible modes would be obtained. Although the authors did not investigate low values of *b/a*, extrapolation of the results from the analysis with values of 7 and 9 indicate that ratios less than 3 would produce roughly equal critical speeds, depending on the thickness of the disk.

Offset Disk

Response with the disk offset from the center of the shaft was mixed. An example of these calculations is illustrated in Figure 7, which is comparable to Figure 2 with just a different value of *x/l*. With the offset, the first mode shows a difference of 26%, with a very minor critical speed discrepancy at the second and third modes.

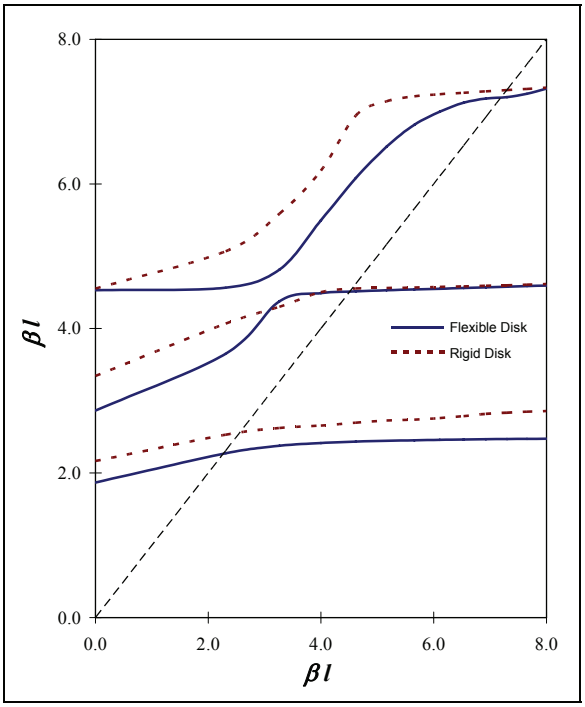

Figure 7. Modes for μ = 1.832, b/a = 7.0, x/l = 0.25

There is not as much critical speed shift with the offset disk due to location. Referring to Figure 8, the mode shapes show that the most rotation of the disk is with the first mode. With the higher modes, the disk is not bending and actually serves as restraint to force the long end of the shaft to deform.

The selection of the *x/l* value equal to 0.25 contributes to the relatively small difference with the second and third modes in another way. Because the deformed shape of the shaft will be sinusoidal, the location ¼ of the way from the ends is roughly at a point of minimum motion for the higher modes. Obviously, other values of this parameter could be used, but a direct comparison to the work of Chivens and Nelson could not have been made.

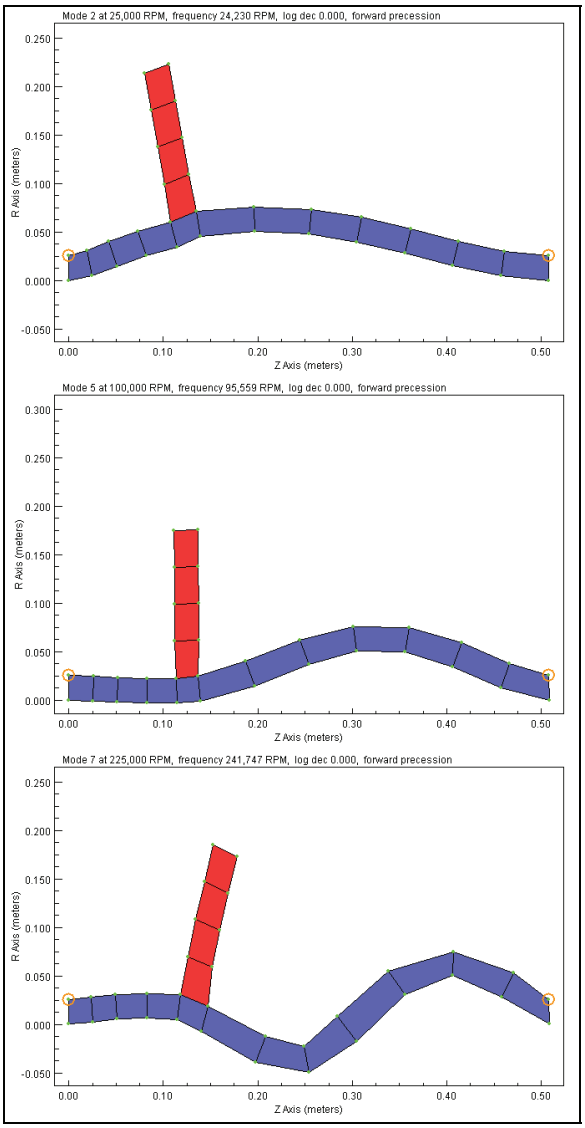

Figure 8. Mode shapes for offset disk

Although not presented in the above results for clarity, the difference between rigid and flexible disk frequencies for backward modes can exceed the separation observed with forward modes. This is consistent with the findings of Chivens and Nelson. While traditionally backward modes are ignored in most rotor dynamic analyses, it is possible to excite these frequencies with support asymmetry.

SUMMARY AND CONCLUSIONS

The application of axisymmetric harmonic finite elements to investigate the effect of disk flexibility on rotor vibration provides a direct and convenient method to assess the influence of this common modeling assumption. Based on the results presented in this paper, the following conclusions can be made:

- There is a significant difference in both natural frequencies and critical speeds with bending mode shapes when disk flexibility is included in the calculations.
- The amount of difference is strongly dependent on the size of the disk and location on the shaft. The thickness of the disk has more of an effect on the frequency difference than the ratio of inner and outer diameters. Placing the disk on the shaft at a location of potentially little bending motion does mitigate the influence of disk flexibility, although this is impractical for any realistic rotor configuration.
- Although this analysis was conducted on a rotor with simply supported end conditions, almost all rotor-bearing systems have some degree of shaft bending and would be influenced by the effects of disk flexibility.

Because of the magnitude of the difference in the critical speeds produced in the analysis conducted in this paper, which was a maximum of 30%, caution is clearly warranted with shaft-disk systems that have very low predicted bending mode margins. As noted by Brémand, Ferraris, and Lalanne, although “it will be necessary to consider the discs as flexible … it is difficult to include” with traditional beam element rotor dynamics programs. The harmonic axisymmetric formulation presented in this paper can directly represent the disk flexibility and offers improved predictions of rotor bending modes.

NOMENCLATURE

a = disk inner radius
A = shaft cross-sectional area
b = disk outer radius
B = element strain-displacement matrix
d = element generalized displacements
D = element constitutive matrix
E = elastic modulus
F, H = terms in D matrix, equation (9)
G = element gyroscopic matrix
I = cross-section inertia
K = element stiffness matrix
l = axial length of shaft
M = element mass matrix
m = harmonic mode number
n = number of nodes per element
N = element shape functions
q = nodal displacements
P = potential energy
r = radial coordinate
T = kinetic energy
u, v, w = radial, axial, and tangential cross-section displacements
V = element volume
x = axial location of disk on shaft
z = axial coordinate
βl = non-dimensional natural frequency,
$= \sqrt[4]{\frac{\omega^2 \rho A}{EI}}\, l$
ε = element strain
γ = element shear strain
Φ = disk flexural rigidity,
$= \frac{Et^3}{12(1-\nu^2)}$ t = disk thickness
μ = shaft-plate stiffness parameter,
$= \frac{\pi \Phi l}{EI}$ EI = shaft stiffness
ν = poisson's ratio
θ = tangential coordinate
ρ = element density
σ = element stress
τ = element shear stress
ω = natural frequency
Ω = element angular velocity

Subscripts

A = anti-symmetric matrix component
e = element matrix
S = symmetric matrix component

REFERENCES

1. Chivens, D. R., and Nelson, H. D., "The Natural Frequencies and Critical Speeds of a Rotating, Flexible Shaft-Disk System," *ASME Journal of Engineering for Industry,* Vol. 97 (1975), pp. 881-886.
2. Dopkin, J.A., and Shoup, T.E., "Rotor Resonant Speed Reduction Caused by Flexibility of Disks," *ASME Journal of Engineering for Industry*, Vol. 96 (1974), pp. 1328-1333.
3. Brémand, P., Ferraris, G., and Lalanne, M., "Prediction of Natural Frequencies of Flexible Shaft-Disc System," *The Shock and Vibration Bulletin, 56th Symposium on Shock and Vibration*, 1986, Vol. II, pp. 71-80.
4. Vance, J. M., Rotordynamics of Turbomachinery, Wiley, 1988, ISBN 0-471-80258-1.
5. Flowers, G.T., "Effects of Rotor Disk Flexibility on the Rotordynamics of the Space Shuttle Main Engine Turbopumps," AIAA Paper 1990-1047, presented at 31st Structures, Structural Dynamics and Materials Conference, Long Beach, CA, Apr 2-4, 1990, contained in AIAA A90-29409 CP, pp. 2206-2213.
6. Greenhill, L. M., Bickford, W. B., and Nelson, H. D., "A Conical Beam Finite Element for Rotor Dynamics Analysis," *ASME Journal of Vibration, Acoustics, Stress, and Reliability in Design*, Vol. 107 (1985), pp. 421-430.
7. Stephenson, R. W., and Rouch, K. E., "Modeling Rotating Shafts using Axisymmetric Solid Finite Elements with Matrix Reduction," *ASME Journal of Vibration and Acoustics,* Vol. 115 (1993), pp. 484-489.
8. Cook, R. D., Malkus, D. S., Plesha, M. E. and Witt, R. J., Concepts and Applications of Finite Element Analysis, Fourth Edition, Wiley, 2002, ISBN 0-471-35605-0.
9. Lund, J. W., and Orcutt, F. K., "Calculations and Experiments on the Unbalance Response of a Flexible Rotor," *ASME Journal of Engineering for Industry,* Vol. 89 (1967), pp. 785-796.